Published in final edited form as:

Ophthalmic Genet. 2021 June ; 42(3): 338–343. doi:10.1080/13816810.2021.1891552.

Multimodal imaging and genetic findings in a case of ARSG-related atypical Usher syndrome

Nicholas Fowler[a], **May El-Rashedy**[a], **Emad Chishti**[a], **Craig W. Vander Kooi**[b], **Ramiro Maldonado**[a]

[a]Department of Ophthalmology and Visual Sciences, University of Kentucky, Lexington, KY

[b]Molecular and Cellular Biochemistry Center for Structural Biology University of Kentucky, Lexington, KY, USA

Abstract

Background: Atypical Usher syndrome has recently been associated with arylsulfatase G (*ARSG)* variants. In these cases, characteristic findings include progressive sensorineural hearing loss (SNHL) without vestibular involvement and ring-shaped late-onset retinitis pigmentosa (RP).

Materials and Methods: One patient with atypical Usher syndrome and a novel homozygous *ARSG* variant was included in this study. The patient underwent a comprehensive ophthalmic examination, including multimodal imaging and genetic testing.

Results: A 60-year-old male of Persian decent presented to our clinic with a history of 20 years of progressive SNHL, and 10 years of progressive peripheral vision loss and pigmentary retinopathy. Consistent with previous reports of *ARSG*-related atypical Usher syndrome, fundus examination revealed ring-shaped retinal hyperpigmentation and fundus autofluorescence (FAF) demonstrated a six-zone pattern of autofluorescence. Optical coherence tomography (OCT) showed extensive cystoid spaces concentrated in the ganglion cell layer. Widefield OCT angiography at the level of the choriocapillaris showed signs of atrophy that corresponded to the FAF hypofluorescent zone. The patient was homozygous for a novel *ARSG* variant c. 1270C>T, p. Arg424Cys.

Conclusion: We report a novel *ARSG* variant in a case of atypical Usher syndrome and describe multimodal imaging findings that further characterize the effect of *ARSG* in the pathogenesis of atypical Usher syndrome.

Keywords

Arylsulfatase G; *ARSG*; Usher syndrome; Usher syndrome type 4; USH4; atypical Usher syndrome; retinitis pigmentosa; RP

Correspondence author: Name: Maldonado, Ramiro, Address: 1110 Conn Terrace, Suite 550, Lexington, KY, 40508, Telephone: 859-216-2627, Fax: 859-257-6718, ramiro.maldonado@uky.edu.

Declaration of interest

The authors report no conflicts of interest. The authors alone are responsible for the content and writing of this article.

Introduction:

Usher syndrome (USH) is a group of ciliopathies characterized clinically by retinitis pigmentosa (RP) and sensorineural hearing loss (SNHL). USH is the leading cause of combined hearing and vision loss, affecting ~400,000 patients worldwide, and has an estimated prevalence as high as 16.7 per 100,000 (1). Usher syndrome is heterogeneous in its genetics and clinical presentation. Recent genetic studies have revealed 16 loci and 13 genes (12 causative, 1 modifier) to be associated with USH (2).

Traditionally, patients with USH have been classified into three subtypes based on symptom onset and severity. USH1 is the most severe form with congenital profound SNHL, vestibular areflexia, and early-onset RP within the first decade of life. USH2, the most prevalent subtype, is characterized by moderate non-progressive SNHL, normal vestibular function, and RP starting as early as adolescence. USH3 presents with progressive SNHL, sometimes accompanied by vestibular dysfunction, and variable onset of RP.

In addition to these classical forms, atypical Usher syndrome is used to describe cases in which the phenotype does not meet the canonical criteria for USH1, USH2, or USH3 (3). To date, atypical Usher syndrome has been associated with eight genes, including *ARSG*. The first report of *ARSG*-related atypical Usher syndrome was described in 2018 by Khateb et al (4). Five patients had late-onset progressive SNHL (18 to 67 years of age) without vestibular involvement and very late-onset RP (42 to 60 years of age) and were all caused by the same *ASRG* variant (c.133G>T, p. Asp45Tyr) which results in loss of enzyme activity (4). In 2020, Abad-Morales et al described a second homozygous missense *ARSG* variant (c. 130G > A, p. Asp44Asn) to be associated with a case of atypical Usher syndrome (5). Here we describe the clinical, multimodal imaging, and genetic findings of a third homozygous missense variant of *ASRG* in a case of atypical Usher syndrome.

Patient and method

The patient was examined in the Ophthalmic Genetics Service at the University of Kentucky. Examination included wide field color fundus photography, fundus autofluorescence (FAF), optical coherence tomography (OCT), OCT angiography (OCTA), Goldmann perimetry, and dilated full-field stimulus threshold testing (D-FST).

Case Report/results

A 60-year-old male of Persian descent was referred to our clinic for retinitis pigmentosa evaluation. On presentation, the patient complained of blurred central vision for 10 years and denied nyctalopia. Ten years before presentation to our clinic, the patient was diagnosed with macular edema (left greater than right eye) for which he was treated bilaterally with prednisolone (1%) drops and later received intravitreal steroids in the left eye. As a result of the steroid therapy in the left eye, he developed a cataract for which he underwent cataract extraction with intraocular lens placement and developed secondary glaucoma for which he received maximal medical therapy for five years. He also reported progressive, moderate-to-severe sensorineural hearing loss since 40 years of age for which he requires bilateral hearing aids. The patient denied symptoms of vestibular dysfunction.

On initial examination, the patient had a best corrected visual acuity of 20/20 and 20/25 in the right and left eyes, respectively. External eye and anterior segment slit lamp examinations were unremarkable except for a 1+ posterior subcapsular cataract in the right eye and a posterior chamber intraocular lens in the left eye. Dilated fundus examination was significant for ring-shaped retinal pigment epithelium (RPE) pigmentary changes encircling the macula that extended temporally to the arcades and nasally past the optic nerve; the RPE pigmentary changes spared the mid- and far-peripheral retina. In addition, the vessels were mildly attenuated in both eyes (Figure 1A). In both eyes, FAF showed a symmetric pattern of six concentric zones (Figure 1B). From central to peripheral, these zones are: zone A, foveal normal fluorescence; zone B, perifoveal hyper-autofluorescence; zone C, normal autofluorescence that extends temporally to the arcades and nasally to the optic nerve head; zone D, hypo-autofluorescence that corresponds to extensive RPE atrophy that does not correlate with the fundus exam findings; zone E, thin hyper-autofluorescence encircling the peripheral edge of zone C; and zone F, normal autofluorescence that extends to the peripheral retina. Retinal thickness maps showed widespread posterior pole retinal thinning that extended from the perifovea to the periphery; the thinned area includes FAF zones C to E, which include zones with normal autofluorescence (Figure 1D).

OCT of the macula showed hyporeflective cystoid spaces predominantly in the ganglion cell layer (GCL) with fewer but larger cystoid spaces in outer (ONL) and inner nuclear layers (INL) as seen in Figure 2 and Table 1. Cystoid spaces were counted across all b-scans (Table 1) and graded per Sahel criteria as moderate edema in the right eye and severe edema in the left eye (6). In addition, OCT showed bilaterally preserved ellipsoid zones and external limiting membranes, and that cystoid spaces were contained within the external limiting membrane (Figure 2C). Finally, in non-foveal areas, there was outer retinal layer atrophy with sparing of the inner retina (Figure 2A); this pattern of retinal thinning was noted from FAF zones C to E.

OCTA revealed many noteworthy findings. First, 3×3mm scans at the level of the superficial capillary (SCP) showed parafoveal capillary flow voids in both eyes (Figure 3A). The flow voids were primarily adjacent to the foveal avascular zone and greater in the left eye. Vessel density of the SCP was 0.32 and 0.35 in the right and left eyes, respectively. In addition, OCTA scans at the level of the deep capillary plexus (DCP) showed a marked decrease of perifoveal capillary flow that spared the fovea (Figure 3B); this demarcation of vessel density corresponds to the retinal thickness demarcation appreciated on the structural thickness map where flow is present only in areas of preserved retinal thickness (Figure 1D). Finally, 12×12mm scans at the level of the choriocapillaris showed underlying choroidal vessels and flow voids, a finding suggestive of atrophy, along the vascular arcades and nasal to the optic nerve that corresponds with fundus exam RPE pigmentary changes and FAF zone D (Figure 3C, D).

Full-field stimulus threshold testing demonstrated a mild subnormal response with −51 and −42 decibels in the right and left eye, respectively. Goldmann perimetry revealed a ring scotoma beyond the central 10 degrees in both eyes.

Genetic testing revealed a novel homozygous missense mutation in the *ARSG* gene (c. 1270C>T, p. Arg424Cys). To date, this variant has not been described in the Genome Aggregation Database or disease-related variation databases such as ClinVar or the Human Genome Mutation Database. Still, the variant is predicted to be damaging by all *in silico* tools, including the Mutation Taster, Sorting Intolerant from Tolerant, and Polymorphism Phenotyping tools. In addition to *ARSG*, our patient had additional variants in genes associated with retinal pathology: *KCNJ13*; *KIAA0586*; *ABCA4*; and *ABHD12.* Importantly, these variants did not fit the phenotype, inheritance mode, or pathogenicity profile of the presented case.

To predict the functional implication of the R424C mutation (c. 1270C>T, p. Arg424Cys), we generated a PHYRE-based homology model, which allows the computational prediction of the structure of an unknown protein using the structure of a known homolog (7). The structure of *ARSG* was modelled using the known structure of the homologous family member arylsulfatase A (*ARSA*) as the template (37% identity/50% homology) with 100% resulting model confidence (8). Examination of the model revealed that R424 is a charged residue integrally located at the subdomain interface, which forms a salt bridge with D76 (Figure 4). Mutation of this residue from arginine to cysteine would thus be deleterious to protein stability due to loss of this specific electrostatic interaction.

Discussion

We present deep phenotyping including multimodal imaging of a case of atypical Usher syndrome caused by a novel homozygous *ARSG* variant. In this report, we describe topographic correlations between fundus photography, autofluorescence, vascular flow and retinal thickness. In addition, we map the retinal cystoid spaces to provide insights into the pathophysiology of this case of atypical Usher syndrome.

The *ARSG* variant reported here has not been previously described in the medical literature or genomic databases. To date, only two papers have reported cases of atypical Usher syndrome related to *ARSG* variants: five patients among three Yemenite Jewish families by Khateb et al and a 44-year-old Spanish female by Abad-Morales et al. Indeed, our patient's phenotype is consistent with these previous reports as they all have late-onset sensorineural hearing loss without vestibular abnormalities and a late-onset retinal involvement that on DFE that showed the ring-shaped retinal atrophy encompassing the vascular arcades temporally and extending nasal to optic nerve with preservation of the mid- and far-periphery (Figure 1). Furthermore, FAF appears similar in all cases with the same concentric six zone pattern of autofluoresence, as described above (Figure 1).

Fundus auto fluorescence zones had interesting correlations with other imaging findings. For example, zone C (normal autofluorescence) correlated with normal choriocapillaris and SCP findings on OCTA, but also with decreased DCP flow on OCTA and decreased retinal thickness. Together, these findings suggest a primary photoreceptor disease with preserved choriocapillaris and retinal pigment epithelium. In addition, the majority of zone D (hypo-autofluorescence) correlated with a patchy pattern of both choriocapillaris flow voids and decreased retinal thickness; in distinction, areas of mild hypo-autofluoresence corresponded

with normal choriocapillaris flow. Together, these findings suggest that choriocapillaris abnormalities follow RPE damage and that FAF may be a more sensitive detector of disease.

OCT revealed cystoid macular edema (CME) in both eyes. In contradistinction, cystoid spaces have not been documented in any previous reports of *ARSG* variants (4,5). Interestingly, the majority of the cystoid spaces were present in the ganglion cell layer (GCL) (85% right eye and 64% left eye; Table 1) which is uncommon for retinitis pigmentosa (RP) associated CME. For example, in one study of 32 eyes with RP CME, only two of the eyes had cysts in the ganglion cell layer (9). In a study of patients with Usher syndrome by Sahel et al, only one of 16 eyes (6%) had cystoid spaces in the GCL (6). In both studies, cystoid lesions tended to concentrate in the INL (6,9). To study this peculiar location of the cystoid spaces, we mapped their axial location in the structural en face image (Figure 2) and found that cystoid spaces were located within an area of preserved external limiting membrane. This confirms that cystoid spaces are present in areas where photoreceptors are best preserved as noted by Makiyama et al (9). In their study of RP associated CME, the cysts were more commonly present inner and/or adjacent to patent external limiting membrane except in cases of vitreomacular traction (9). In addition, they found vitreomacular traction and epiretinal membranes to be highly associated with the presence of cystoid spaces but not related to the location of cystoid spaces. In our case, we show that the right eye has a greater area of vitreo-macular attachment while the left eye has more severe cystoid lesions. These findings suggest a more pronounced tractional force per area in the left eye is responsible for the greater number and size of cystoid spaces. In addition, OCT demonstrated the GCL cavitary spaces tended to be vertically elongated and that inter-cystoid spaces had hyperreflective vertical pillars. These hyperreflective pillars are thought to represent swollen Müller fibers in cases of retinal degenerative CME; oxidative stress and inflammation lead to Müller cell disruption with subsequent intracellular K+ overload and reduced water efflux which ultimately results in Müller cell swelling (10).

In contrast to a report from Yeo et al (11) that describes OCTA findings in eyes with RP associated CME, OCTA analysis showed that flow voids coincided with cystoid lesions. Specifically, nearly all SCP focal parafoveal flow voids overlapped with cystoid space, but not all cystoid spaces overlapped with focal flow voids. The authors question if these flow voids are truly devoid of flow from a potential cystic compressive effect or if the no signal areas are the result of segmentation error caused by the lesions. In vasculogenic CME, as in cases of diabetic macular edema and retinal branch vein occlusion, loss of capillary integrity results in vascular disruption and capillary dropout; in these cases, DCP flow voids are invariably present in spaces with cystoid lesions (12). The flow voids can be larger or smaller than the accompanying cystoid space.

The above-described structural findings were confirmed on the functional level through Goldmann perimetry and full-field stimulus threshold testing. Goldmann perimetry showed a ring scotoma that corresponded to the FAF ring of RPE atrophy. The mildly subnormal FST response, absence of nyctalopia, and large area of normal autofluorescence suggest that a good proportion of the retina is still preserved.

In silico tools predict that the identified homozygous variant (Arg424Cys) would be pathogenic. Previous reported mutations in *ARSG* are located in the enzyme active site and result in loss of enzyme activity (4,5). R424, the amino acid and primary structure sequence effected by the mutation, is strictly conserved in vertebrate orthologs of *ARSG* (Figure 4). This new mutation expands the regions of *ARSG* implicated in disease and may define a novel site of mutational sensitivity. Intriguingly, this region of the enzyme may prove to be critical for stability in the broader sulfatase family, since *ARSA* mutations at the equivalent position (Arg390Gln and Arg390Trp) have been reported to be causative of metachromatic leukodystrophy (13).

In this study, we report a novel *ARSG* missense mutation (c. 1270C>T, p. Arg424Cys) identified in a case of atypical Usher syndrome. This is predicted to change the amino acid arginine to cysteine at position 424, thereby producing a phenotype consistent with previously reported cases related to *ARSG* mutations. We enhance the characterization of the *ARSG*-related atypical Usher syndrome cases with deep multimodal imaging phenotyping and the use of functional testing such as full-field threshold.

Acknowledgements

The authors would like to acknowledge the Foundation Fighting Blindness My Retina Tracker Registry for their financial support in genetic testing.

Funding Disclosure Statement

This work was supported in part by the National Institutes of Health (NIH) under award number R01DC019054 (to C.W.V.K). The content is solely the responsibility of the authors and does not necessarily represent the official views of the National Institutes of Health. This work was also supported in part by the Foundation Fighting Blindness My Retina Tracker Registry.

References

1. Kimberling WJ, Hildebrand MS, Shearer AE, et al. Frequency of Usher syndrome in two pediatric populations: implications for genetic screening of deaf and hard of hearing children. Genet Med. 2010; 12(8):512–16. doi:10.1097/GIM.0b013e3181e5afb8. [PubMed: 20613545]
2. Mathur P, Yang J Usher syndrome: hearing loss, retinal degeneration and associated abnormalities. Biochim Biophys Acta. 2014; 852(3):406–420.
3. Nolen RM, Hufnagel RB, Friedman TB, et al. Atypical and ultra-rare Usher syndrome: a review. Ophthalmic Genet. 2020;41(5):401–412. [PubMed: 32372680]
4. Khateb S, Kowalewski B, Bedoni N, et al. A homozygous founder missense variant in arylsulfatase G abolishes its enzymatic activity causing atypical Usher syndrome in humans. Genet Med. 2018;20(9):1004–1012. [PubMed: 29300381]
5. Abad-Morales V, Navarro R, Burés-Jelstrup A, et al. Identification of a novel homozygous mutation as the second cause of Usher syndrome type 4. Am J Ophthalmol Case Rep. 2020; 19:100736. [PubMed: 32455177]
6. Sliesoraityte I, Peto T, Mohand-Said S, Sahel JA. Novel grading system for quantification of cystic macular lesions in Usher syndrome. Orphanet J Rare Dis. 2015;10:157. [PubMed: 26654877]
7. Kelley L, Mezulis S, Yates C et al. The Phyre2 web portal for protein modeling, prediction and analysis. Nat Protoc 10, 845–858 (2015). [PubMed: 25950237]
8. Lukatela G, et al. (1998). “Crystal Structure of Human Arylsulfatase A: The Aldehyde Function and the Metal Ion at the Active Site Suggest a Novel Mechanism for Sulfate Ester Hydrolysis.” Biochemistry 37(11): 3654–3664. [PubMed: 9521684]

9. Makiyama Y, Oishi A, Otani A, et al. Prevalence and spatial distribution of cystoid spaces in retinitis pigmentosa: investigation with spectral domain optical coherence tomography. Retina. 2014;34(5):981–8. [PubMed: 24756036]

10. Chung Y-R, Kim YH, Lee SY, Byeon H-E, Lee K. Insights into the pathogenesis of cystoid macular edema: leukostasis and related cytokines. Int J Ophthalmol. 2019;12(7):1202–1208. [PubMed: 31341814]

11. Yeo JH, Kim YJ, Yoon YH. Optical coherence tomography angiography in patients with retinitis pigmentosa-associated cystoid macular edema. Retina. 2020.

12. Spaide RF. Volume-Rendered Optical Coherence Tomography of Diabetic Retinopathy Pilot Study. Am J Ophthalmol. 2015;160(6):1200–1210. [PubMed: 26384548]

13. Lugowska A, Płoski R, Włodarski P, Tylki-Szymańska A. Molecular bases of metachromatic leukodystrophy in Polish patients. J Hum Genet. 2010;55(6):394–396. [PubMed: 20339381]

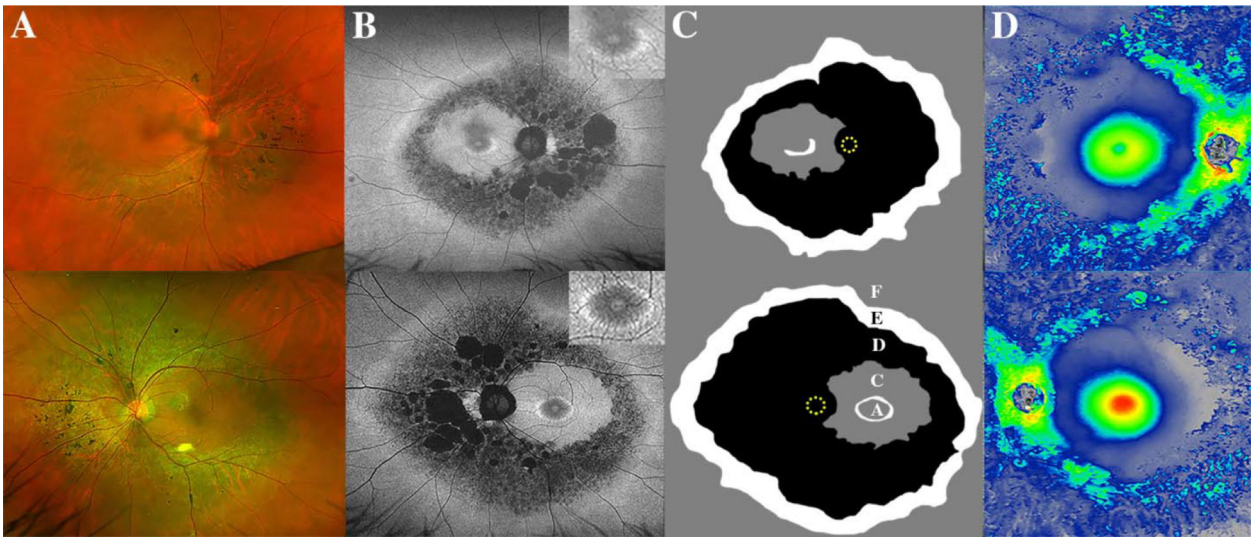

Figure 1.

Retinal imaging of right (top row) and left (bottom) eyes. (a) Color fundus photography shows sharply demarcated pigmentary changes in the posterior pole. (b) Fundus autofluorescence shows a concentric zone pattern that includes the foveal region (inset). (c) Fundus autofluorescence zone pattern (labeled) represented by black (hypofluoresence), white (hyperfluorescence), and grey (normal fluoresence) zones; yellow circle represents optic nerve head. (d) 12×12mm thickness maps show retinal thinning with foveal sparing.

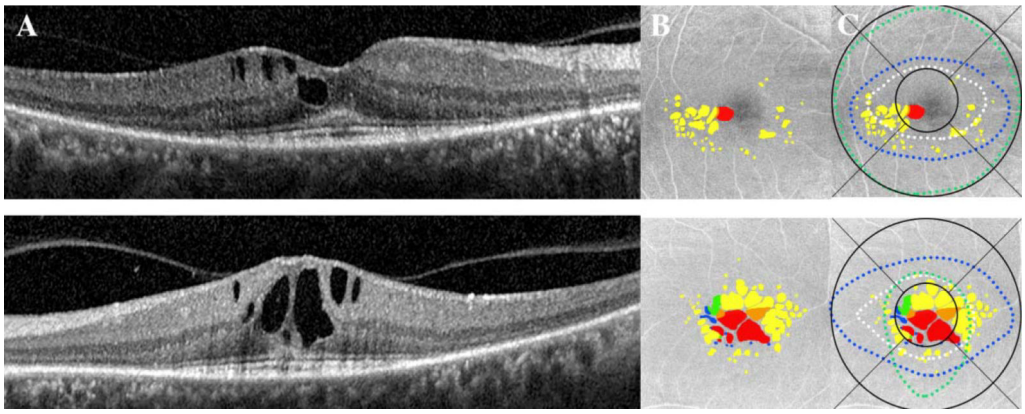

Figure 2.

Cystoid space analysis in the right (top) and left (bottom) eyes. (a) Optical coherence tomography b-scan at the foveal center shows vertically elongated cystoid lesions that were most prevalent in the ganglion cell layer and separated by hyperreflective tissue. (b) En face slabs of structural OCT show the topographical location of the cystoid space in axial and transverse positions. In the axial plane, yellow indicates cystoid spaces in GCL; red, in INL; blue, in ONL; orange, in GCL and INL; and green, in GCL and ONL. (c) En face structural OCT with ETDRS grid overlay and outlines of ellipsoid zone band (white), external limiting membrane (blue), and vitreomacular attachment (green).

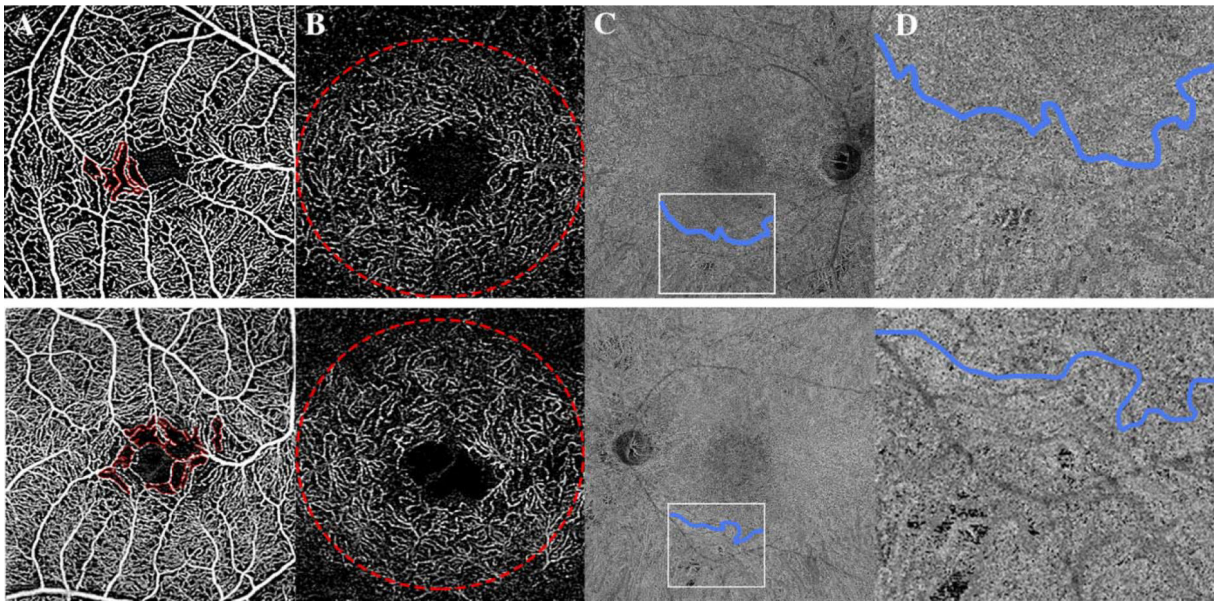

Figure 3.

Optical coherence tomography angiography findings in the right (top) and left (bottom) eyes. (a) 3×3mm scans of the superficial capillary plexus show area of parafoveal capillary flow voids (outlined in red). (b) 3×3mm scans of the deep capillary plexus show perifoveal flow voids, as illustrated outside of the red circle. (c, d) 12×12mm scans of the choriocapillaris show areas of normal flow (above blue line) and scattered flow voids (below blue line) that correspond to fundus normal- and hypo-autofluorescence, respectively.

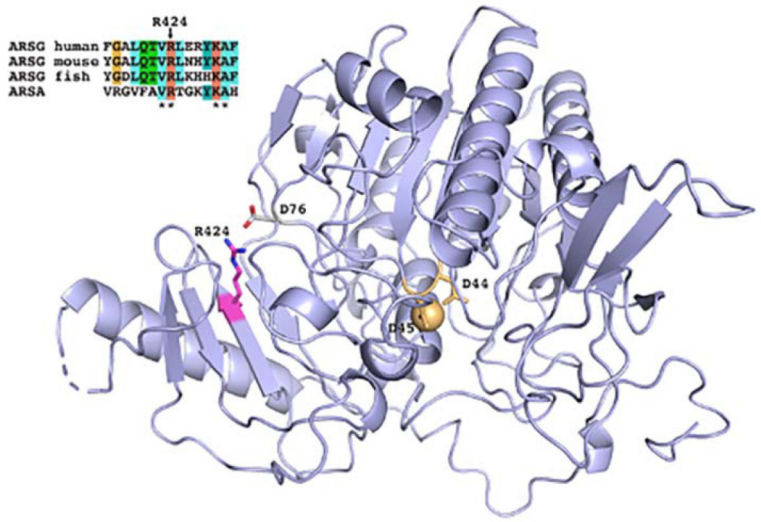

Figure 4.

Homology model of ARSG reveals the location and interactions of key residues mutated in cases of ARSG-related atypical Usher syndrome. R424 is the amino acid residue effected by the described variant; D44 and D45 are residues which are predicted to chelate the divalent cation (tan sphere) in the enzyme active site, described in previous reports of ARSG-related atypical Usher syndrome. Multiple sequence alignment and conservation of ARSG R424 in different species and between ARSG and ARSA (inset). Graphics were prepared with Pymol (www.pymol.org).

Table 1.

Axial location of cystoid lesions on optical coherence tomography

	Right eye	Left eye
Cyst location		
GCL, n (%)	21 (84%)	41(64%)
INL, n (%)	3 (12%)	12 (19%)
ONL, n (%)	1 (4%)	11 (17%)

GCL, ganglion cell layer; INL, inner nuclear layer; ONL, outer nuclear layer.